PDZ Ligand Binding-Induced Conformational Coupling of the PDZ–SH3–GK Tandems in PSD-95 Family MAGUKs

Menglong Zeng[1,†], **Fei Ye**[1,2,†], **Jia Xu**[1,†] **and Mingjie Zhang**[1,2]

1 - Division of Life Science, *State Key Laboratory of Molecular Neuroscience, Hong Kong University of Science and Technology, Clear Water Bay, Kowloon, Hong Kong, China*
2 - Center of Systems Biology and Human Health, *Hong Kong University of Science and Technology, Clear Water Bay, Kowloon, Hong Kong, China*

Correspondence to Mingjie Zhang: *Division of Life Science, State Key Laboratory of Molecular Neuroscience, Hong Kong University of Science and Technology, Clear Water Bay, Kowloon, Hong Kong, China. mzhang@ust.hk*
https://doi.org/10.1016/j.jmb.2017.11.003
Edited by Ichio Shimada

Abstract

Discs large (DLG) MAGUKs are abundantly expressed in glutamatergic synapses, crucial for synaptic transmission, and plasticity by anchoring various postsynaptic components including glutamate receptors, downstream scaffold proteins and signaling enzymes. Different DLG members have shared structures and functions, but also contain unique features. How DLG family proteins function individually and cooperatively is largely unknown. Here, we report that PSD-95 PDZ3 directly couples with SH3–GK tandem in a PDZ ligand binding-dependent manner, and the coupling can promote PSD-95 dimerization and multimerization. Aided by sortase-mediated protein ligation and selectively labeling, we elucidated the PDZ3/SH3–GK conformational coupling mechanism using NMR spectroscopy. We further demonstrated that PSD-93, but not SAP102, can also undergo PDZ3 ligand binding-induced conformational coupling with SH3–GK and form homo-oligomers. Interestingly, PSD-95 and PSD-93 can also form ligand binding-induced hetero-oligomers, suggesting a cooperative assembly mechanism for the mega-*N*-methyl-D-aspartate receptor synaptic signaling complex. Finally, we provide evidence showing that ligand binding-induced conformational coupling between PDZ and SH3–GK is a common feature for other MAGUKs including CASK and PALS1.

Introduction

A characteristic feature of the excitatory synapse is the postsynaptic density (PSD), a specialized electron-dense region located at the tip of the dendritic spine and underneath the postsynaptic plasma membranes [1]. A wide variety of molecules including glutamate receptors, adhesion molecules, ion channels, scaffolding proteins, cell signaling proteins and cytoskeleton-related proteins are condensed in the PSD, allowing for efficient response to and processing of signals transmitted by presynaptic glutamate releases [2–5]. Among them, scaffold proteins serve as organizational platforms to anchor and assemble other PSD components.

Discs large (DLG) family scaffold proteins are a class of the membrane-associated guanylate kinases (MAGUKs) and have been long recognized as the central PSD scaffold proteins [5–8]. DLG MAGUKs include four paralogs in mammals, DLG1–4 (also known as synapse-associated protein (SAP)97/hDLG [9], PSD-93/Chapsyn-110 [10,11], SAP102 [12] and PSD-95/SAP90 [13,14], respectively), via two rounds of genome duplications throughout the evolution. All four DLGs share a high-amino-acid sequence identity and a very similar modular structural organization consisting of three PDZ domains at the N-terminal half and a SH3–GK tandem at the C-terminal half. The PDZ domains of all four DLGs have been shown to interact directly with *N*-methyl-D-aspartate (NMDA) receptors and to bind to α-amino-3-hydroxy-5-methyl-4-isoxazolepropionic acid (AMPA) receptor directly or indirectly via its auxiliary subunits transmembrane AMPAR regulatory proteins (TARPs) [15–19]. The SH3–GK tandem of DLGs folds into structurally similar supramodules and shares similar target binding

properties [20–22]. The high sequence and structural similarities among the members of DLGs are reflected in their functional redundancies. For example, germ-line knockout of PSD-95 in mice has little impact on the synaptic transmission [23,24], presumably due to compensatory effect by other members of DLGs. Simultaneous and acute removal of multiple DLGs (PSD-95, PSD-93 and SAP102) both in slice cultures and in dissociated neurons via a chained miRNA-mediated knock-down approach led to dramatic losses of both AMPAR and NMDAR transmissions as well as decreases of PSD volumes [25,26], indicating that DLGs are key architectural proteins responsible for both anchoring glutamate receptors at synapses and for overall organization of the PSD. However, as one would expect, the four members of DLGs each have their own sequence features, which presumably account at least in part for the unique functional properties of each DLGs. For example, the N-terminal ends of PSD-95 and PSD-93 can be palmitoylated, and palmitoylation regulates PSD-95's synaptic targeting and stability [27,28]. SAP97 is not known to contain any palmitoylation site [27]. Instead, SAP97 contains an L27 domain at its N-terminal end, and this L27 domain determines SAP97's binding partners via formation of L27 hetero-tetramers with cell polarity regulatory proteins such as protein associated with Lin-7 1 (PALS1) and MALS [29,30]. Fittingly, SAP97 is universally required for cell polarity development and maintenance in essentially all tissues including neurons [9], whereas PSD-95, PSD-93 and SAP102 (but not SAP97) are required for basal synaptic transmissions [23,25]. Although each paralog of PSD-95, PSD-93 and SAP102 contributes to basal synaptic transmissions and to PSD formation with apparent redundant mechanisms [23,25], each member of these three DLGs plays distinct cognitive functions [31]. It was recently shown that PSD-95 and PSD-93 are mutually dependent on each other to form a highly stable NMDAR-containing complex assembly with a molecular mass of ~1.5 MDa [32], although the molecular basis governing such large NMDAR complex assembly is unclear. The expansion of the DLG family members through the whole-genome duplications along the evolution presumably increases the functional diversity of DLGs in mammals with respect to invertebrates, which typically contain only one DLG member in their genomes. However, very little is known regarding how different members of DLGs in mammals may function both cooperatively and differently. This is especially true with regard to the common domains (i.e., the PDZ domains and the SH3–GK tandem) among DLGs.

The multi-domain organization feature renders DLGs ideal for integrating various synaptic signaling pathways. Since each domain in DLGs can typically fold and bind to different partner proteins, these domains are often treated as structurally and functionally independent modules tethered by flexible linkers (i.e., the so-called “beads on a string” model). However, it is increasingly recognized that, in addition to function individually, multiple domains within a scaffold protein can often interact with each other forming structural supramodules with cellular functions distinct from each individual domains or simple sum of these individual domains [33,34]. For example, all MAGUKs except for MAGIs share a common PDZ–SH3–GK (P-S-G) tandem at their C-terminal ends [5]. The P-S-G tandems in several MAGUKs have been shown to function as structural and functional supramodules in the past few years. Structural studies of the P-S-G tandems from PALS1 and ZO-1, both in complex with their specific binding peptides, showed that the three domains in each P-S-G tandem physically interact with each other forming an integral structural unit necessary for specific target protein bindings [35–37]. The structure of the PALS1 P-S-G in complex with the Crumbs tail peptide further suggests a possible multimerization mechanism for MAGUK P-S-G tandems [35]. Earlier biophysical studies have indicated that the PDZ3 of PSD-95 can transiently interact with the SH3–GK module [38,39]. We recently demonstrated that the P-S-G tandem of PSD-95 can bind to SynGAP with a ~10-fold higher affinity than the extended PDZ3 domain [40], suggesting that the P-S-G tandem of PSD-95 may also form a supramodule. We further provided evidence that the P-S-G tandem of PSD-95 can undergo SynGAP binding-induced multimerization, although with an unclear mechanism [40]. Nonetheless, our previous study points to the following exciting possibilities of the DLG subfamily MAGUKs. (*i*) The PDZ3 domain and the SH3–GK tandem of DLGs may conformationally couple with each other, and such coupling is mediated by the target binding to the PDZ3 domain. (*ii*) The SynGAP binding-induced multimerization of PSD-95 P-S-G tandem suggests that DLGs may also be able to form hetero-oligomers in addition to homo-multimers. Formation of DLG hetero-oligomers could provide a mechanistic explanation for cooperative actions of DLGs in organizing NMDAR signaling complexes in the PSD. (*iii*) Possible formations of oligomers via combinations of different DLG paralogs may further expand the functional diversity of DLG-assembled signaling complexes in synapses. (*iv*) Ligand binding-induced conformational coupling may also occur in other MAGUK P-S-G tandems.

Here, we develop a selectively labeling approach, together with NMR spectroscopy, to study the molecular mechanism governing the conformational coupling between the PDZ and the SH3–GK unit in the DLG P-S-G tandems. We discover that the PDZ and SH3–GK conformational coupling is specific to PSD-95 and PSD-93 and does not occur in SAP102. We further show that the GK domain determines the P-S-G coupling in DLGs. Finally, we demonstrate that PDZ ligand binding-induced P-S-G tandem coupling also occurs in other MAGUKs including calcium/

calmodulin-dependent serine protein kinase (CASK) and PALS1.

Results

SynGAP induces PSD-95 PDZ3-C/SH3–GK coupling

We previously showed that PSD-95 PDZ3 contains an elongated C-terminal α-helix (residues 394P–414S, highlighted in yellow in Fig. 1a as αC-helix) that specifically recognizes the extended PDZ binding motif from the SynGAP α1 C-terminal tail (referred to as SynGAP E-PBM hereafter). Chemical crosslinking experiment captured the SynGAP E-PBM binding-induced PSD-95 PDZ3–SH3–GK (P-S-G) tandem dimerization [40], although the detailed mechanism underlying the SynGAP-induced PSD-95 P-S-G dimerization was unclear.

We purified TRX-tagged PDZ3-C (residues 309R-415S; details of key constructs used in the study are listed in a table in Methods) and SH3–GK (residues 422S-724L) both with very high purity and homogeneity. Analytical gel filtration chromatography showed that PDZ3-C alone has no detectable interaction with SH3–GK (pink curve in Fig. 1b). Interestingly, PDZ3-C mixed with two molar ratios of a synthetic peptide comprising of the last 15 residues of SynGAP (SynGAP 15AA) shows a direct binding to SH3–GK, as the PDZ3-C/SH3–GK mixture in the presence of SynGAP 15AA displays an obvious peak shift toward a smaller elution volume than the mixture without SynGAP (blue curve *versus* pink curve, Fig. 1b). Isothermal titration calorimetry (ITC)-based binding assay directly confirmed that the PDZ3-C/15AA complex binds to SH3–GK with a dissociation constant (K_d) around 42.0 μM (Fig. 1c). It is expected that binding between the SynGAP peptide saturated PDZ3-C and SH3–GK would be considerably stronger when the two segments are existing as a single chain in the native PSD-95.

PDZ3-C/SH3–GK coupling promotes P-S-G dimerization

We purified PSD-95 P-S-G tandem (residues 309R-724L) and characterized its hydrodynamic properties by analytical ultracentrifugation (AUC) analysis. Without SynGAP 15AA, PSD-95 P-S-G displays a relatively sharp peak with a monomer molar mass in the sedimentation velocity analysis (red curve, the measured molar mass of 52.9 kDa *versus* the theoretical mass of 47.0 kDa) (Fig. 1d). In the presence of two molar ratios of SynGAP 15AA, PSD-95 P-S-G/15AA shows a broader peak with a fitted molar mass of ~107 kDa (blue curve) (Fig. 1d). The theoretical molar mass of PSD-95 P-S-G in complex with 15AA is around 48.8 kDa (47.0 kDa + 1.8 kDa). The measured molar mass of the P-S-G/15AA complex matches well with a dimeric assembly of the P-S-G tandem. The broad shape of the P-S-G/15AA complex may imply the existence of multiple assembly modes (e.g., monomer, dimer, and oligomers) of the complex interconverting at fast time scales. The somewhat asymmetric complex peak shape (i.e., tailing of the peak at high sedimentation coefficient values) also suggests the existence of multimerized P-S-G/15AA complex in the mixture (Fig. 1d). The oligomeric P-S-G assemblies of the P-S-G/15AA complex were also captured by our earlier chemical crosslinking experiment [40]. Finally, we used fast protein liquid chromatography coupled with static light scattering (FPLC–SLS) analysis to investigate SynGAP binding-induced P-S-G multimerization. Again, apo-PSD-95 P-S-G is a homogenous monomer in solution (red curve in Fig. 1e). Binding of SynGAP 15AA shifts the complex peak toward smaller elution volume and with a larger apparent molar mass (blue curve in Fig. 1e). The SLS measured molar mass of P-S-G/15AA complex is between a monomer and a dimer, which likely reflects an average molecular mass of multiple forms of the complex rapidly exchanging during the elution on the gel filtration column.

PDZ3-C/SH3–GK coupling enhances PSD-95's binding to SynGAP

Interactions between many isolated PDZ domains and their ligands are often weak (K_d of a few to tens of micromolars) and promiscuous [41]. P-S-G tandems in other MAGUK proteins have been reported to have higher binding affinities and specificities in their ligand recognitions than their isolated PDZ domains [35]. We used ITC to compare the binding affinities of the isolated PDZ3-C domain and P-S-G tandem of PSD-95 in binding to SynGAP 15AA peptide. PDZ3-C binds to SynGAP 15AA with a K_d of ~4.0 μM (Fig. 1f, left panel). The P-S-G tandem binds to SynGAP 15AA with a K_d of ~0.5 μM, which is about 8-fold stronger than the isolated PDZ3-C (Fig. 1f). To make sure that the measured affinity increasing is resulted from the binding enhancement afforded by the P-S-G tandem instead of the dimerization of P-S-G, we performed a competition experiment using analytical gel filtration chromatography. When purified PSD-95 P-S-G, TRX-PDZ3-C, and SynGAP C-terminal coiled-coil-PBM fragment (CC-PBM; [40]) were mixed at a 1:1:1 ratio, we only observed the formation of the CC-PBM/P-S-G complex. No obvious CC-PBM/TRX-PDZ3-C complex peak was detected (Fig. 1f), indicating that the P-S-G tandem indeed has a stronger affinity in binding to SynGAP than PDZ3-C does. Supporting the ITC results, the size exclusion column-based experiments demonstrate that P-S-G can efficiently compete with PDZ3-C to form a stable

complex with SynGAP CC-PBM, suggesting that P-S-G has a stronger binding to SynGAP C-terminus than PDZ3-C does (Fig. 1g). Therefore, in addition to mediating dimerization, PDZ3-C/SH3–GK coupling also enhances the PSD-95/SynGAP complex formation.

Segmental labeling of PSD-95 P-S-G by sortase-mediated protein ligation

To understand the molecular basis governing the ligand-induced PSD-95 PDZ3-C/SH3–GK coupling, we have extensively screened PSD-95 P-S-G/SynGAP E-PBM complex crystals but so far with no success. The dynamic exchanges of multiple assembly modes indicated by the AUC analysis (Fig. 1d) might have hampered crystal growth of the complex. We resorted to NMR spectroscopy for possible solutions. Another reason for choosing NMR spectroscopy is that the method is particularly suited for investigating dynamic conformational coupling of proteins and protein complexes. However, for large multi-domain proteins like PSD-95 P-S-G, the complexity of NMR spectra often imposes practical

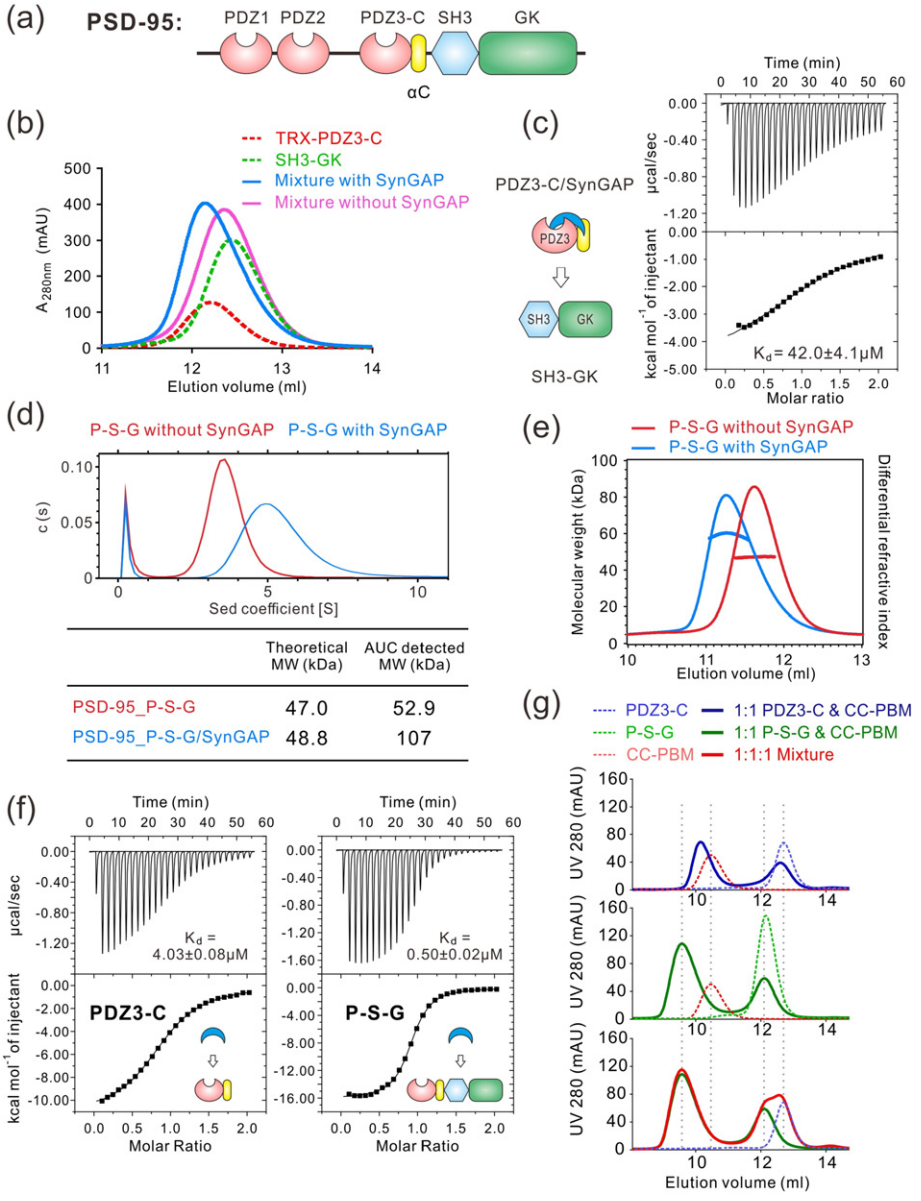

Fig. 1 (*legend on next page*)

challenges for detailed analysis of conformational changes/couplings. One way to overcome such challenge is to only label a selected portion of protein with stable isotopes that are observable by NMR spectroscopy.

We opted to sortase-mediated protein ligation method [42] for selective labeling desired segment (either PDZ3-C or SH3–GK) of PSD-95 P-S-G by ^{15}N. Sortase ligation site was selected at the flexible linker between PDZ3-C and SH3–GK with the sequence of ^{416}LGSGTA^{421} (Fig. 2a). We first replaced the native "LGSGTA" sequence at the tail of PDZ3-C with the sortase-compatible "LPETGG" and added a "GG" cap to the SH3–GK protein (Fig. 2a). Sortase-mediated ligation will result in a covalently linked PDZ3-C–SH3–GK protein, within which only 5 residues in the flexible PDZ3–SH3 linker region (^{417}GSGTA^{421}) replaced by another 5-residue fragment ("PETGG") with similar flexible structural properties (Fig. 2a). Therefore, it is predicted that this sortase-ligation strategy would introduce minimal conformational alterations to PSD-95 P-S-G, but allow us to selectively ^{15}N-label either PDZ3-C or SH3–GK for NMR-based structural studies of the P-S-G tandem in solution.

The success of the above segmental labeling design is demonstrated by comparing the ^{1}H,^{15}N heteronuclear single quantum coherence (HSQC) spectra of the overall ^{15}N-labeled PSD-95 P-S-G (^{15}N_PDZSH3GK) and segmentally ^{15}N-labeled P-S-G samples (^{15}N_PDZ–^{14}N_SH3GK and ^{14}N_PDZ–^{15}N_SH3GK) (see Fig. 2b for the definition of samples). The peaks from ^{15}N_PDZ–^{14}N_SH3GK (or from ^{14}N_PDZ–^{15}N_SH3GK) overlap with a subset of peaks within the fully ^{15}N-labeled P-S-G (Figs. 2c and S1). The merged spectra of ^{15}N_PDZ–^{14}N_SH3GK and ^{14}N_PDZ–^{15}N_SH3GK perfectly overlap with the spectrum of the fully ^{15}N-labeled P-S-G (Fig. 2d), indicating that the sortase-ligated P-S-G retains its native conformation. In this way, the simplified NMR spectra of both ^{15}N_PDZ–^{14}N_SH3GK and ^{14}N_PDZ–^{15}N_SH3GK samples permitted us for detailed analysis of the PDZ3-C/SH3–GK coupling at the individual residue resolution as detailed below. We have also compared the SynGAP binding affinities of the sortase-ligated P-S-G and the wild-type P-S-G, and found that the two versions of P-S-G have essentially the same SynGAP binding affinity (data not shown).

The segmental labeling strategy allowed us to selectively monitor the conformational changes of PDZ3-C upon SynGAP 15AA binding to P-S-G. Titrating of the SynGAP 15AA peptide to ^{15}N_PDZ–^{14}N_SH3GK resulted in a dose-dependent gradual disappearance of the peaks corresponding to the apo-PDZ3-C part and appearance of a new set of peaks corresponding to the peptide bound PDZ3-C of P-S-G (Fig. 3a). This slow timescale exchange between apo- and SynGAP peptide-bound forms of P-S-G is consistent with the sub-micromolar dissociation constant of the complex shown in Fig. 1f. In addition to the chemical shift changes, the peak intensities of ^{15}N_PDZ–^{14}N_SH3GK saturated with the SynGAP peptide are dramatically decreased (by more than 70%) when compared to the apo-protein (Figs. 3a and S2A). Based on the SynGAP peptide binding-induced dimerization observed in biochemical characterizations (Fig. 1), we believed that the peak broadening is largely due to the PDZ3-C/SH3–GK coupling-induced P-S-G dimerization. The SynGAP peptide binding-induced peak broadening may also arise from the dynamic exchange between peptide-bound and peptide-free forms of ^{15}N_PDZ–^{14}N_SH3GK. However, this is unlikely to be true for this case, as titration of the SynGAP peptide into isolated ^{15}N-PDZ3-C resulted in minimal peak broadening (Fig. S2B). If the peak broadening observed for PDZ3-C results from the SynGAP peptide binding-induced P-S-G multimerization, one should be able to observe concomitant peak intensity decrease of the SH3–GK part if using the ^{14}N_PDZ–^{15}N_SH3GK sample for the titration experiment. Indeed, the binding of the SynGAP peptide caused similar dramatic peak

Fig. 1. SynGAP 15AA binding-induced PSD-95 PDZ3-C/SH3–GK coupling. (a) Schematic diagram showing the domain organization of PSD-95. A C-terminal helical extension of PDZ3 (αC, in yellow) is critical for the specific recognition of SynGAP by PSD-95. (b) Analytical gel filtration chromatography showing the SynGAP 15AA binding-induced direct coupling between PSD-95 PDZ3-C and SH3–GK (100 μM TRX-PDZ3-C, 100 μM SH3–GK-His, 200 μM SynGAP 15AA peptide). (c) ITC titration profile showing the binding between SynGAP 15AA-saturated PSD-95 PDZ3-C and PSD-95 SH3–GK. TRX-PDZ3-C (at 1 mM mixed with 1.2 mM SynGAP 15AA peptide) was titrated into SH3–GK-His (at 100 μM) in the cell. (d) AUC analysis showing the SynGAP 15AA binding-induced PSD-95 P-S-G dimerization/multimerization. The fitted molecular masses are presented in the table at right. (e) FPLC–SLS analysis showing the SynGAP 15AA binding-induced PSD-95 P-S-G multimerization. (f) ITC titration profiles showing that PSD-95 P-S-G (right panel; 300 μM SynGAP 15AA peptide was titrated to 30 μM P-S-G in the cell) binds to SynGAP with a higher affinity than PDZ3-C does (left panel; 400 μM SynGAP 15AA peptide was titrated into 40 μM TRX-PDZ3-C in the cell). (g) Analytical gel filtration-based competition experiment indicates that PSD-95 P-S-G, in the presence of equal molar amount of PDZ3-C, preferentially binds to SynGAP (bottom panel). The top and middle panels show that PDZ3-C and P-S-G can individually form complex with SynGAP on gel filtration column. The concentration of the proteins used in the experiment is 50 μM.

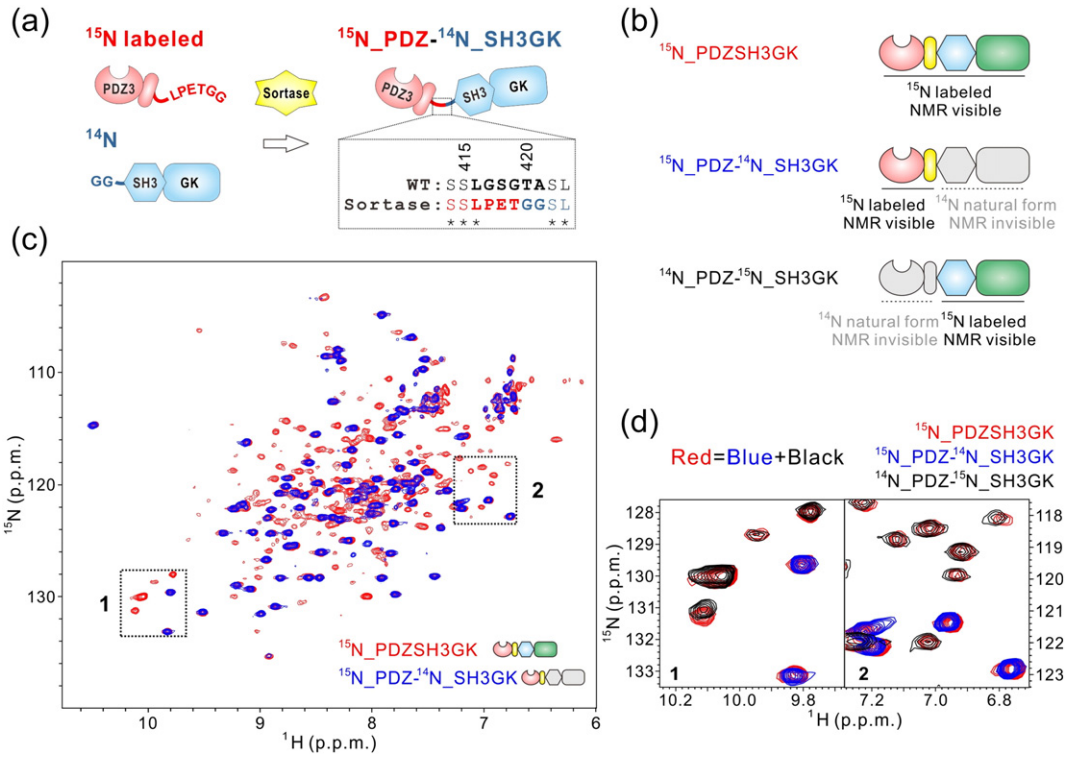

Fig. 2. Sortase-mediated selective segmental ^{15}N-labeling of PSD-95 P-S-G. (a) Schematic diagram showing that ^{15}N-labeled PDZ3-C with a C-terminal "LPETGG" tail is covalently ligated to an N-terminal "GG"-capped ^{14}N SH3–GK. The reaction was catalyzed by sortase. Compared to the wild-type P-S-G, the sortase-ligated P-S-G does not alter the length of the protein and only introduces five-residue change in the flexible PDZ3–SH3 linker region. (b) Schematic diagram showing various domain-selectively ^{15}N-labeled PSD-95 P-S-G samples used for the NMR analysis. (c) Superposition plot of ^{1}H,^{15}N HSQC spectra of uniformly ^{15}N-labeled PSD-95 P-S-G (red peaks) and PDZ3-C selectively ^{15}N-labeled P-S-G (blue peaks). Two black dotted rectangles are expanded in panel D. (d) Superposition plots of two selected regions of ^{1}H,^{15}N HSQC spectra of uniformly ^{15}N-labeled P-S-G (red peaks), PDZ3-C ^{15}N-labeled P-S-G (purple peaks) and SH3–GK ^{15}N-labeled P-S-G (black peaks), showing that sortase-ligated P-S-G has the same conformation as the native protein. Also see Fig. S1.

Fig. 3. NMR spectroscopic studies showing the mechanism of the SynGAP binding-induced PSD-95 P-S-G supramodule formation. (a) A selected region of ^{1}H,^{15}N HSQC–TROSY spectra of PSD-95 ^{15}N_PDZ–^{14}N_SH3GK used to show the titration of the sample with the SynGAP 15AA peptide (full spectra are shown in Fig. S2A). The average peak intensity of the PDZ domain is quantified and presented using bar diagram at right. The positions of three peaks corresponding to apo- ^{15}N_PDZ–^{14}N_SH3GK are highlighted with dotted circles in red. (b) A selected region of ^{1}H, ^{15}N HSQC–TROSY spectra of PSD-95 ^{14}N_PDZ–^{15}N_SH3GK used to show the titration of the sample with the SynGAP 15AA peptide (full spectra are shown in Fig. S2C). (c) Superposition plot of two selected regions of ^{1}H,^{15}N HSQC–TROSY spectra of ^{15}N-PDZ3-C saturated with SynGAP 15AA (red) and of ^{15}N_PDZ–^{14}N_SH3GK saturated with SynGAP 15AA (blue peaks). The full spectra are shown in Fig. S3B. The assignments of the peaks corresponding to the ^{15}N-PDZ3-C/SynGAP 15AA complex are labeled. (d) Mapping of the backbone amide chemical shift changes of PDZ3-C resulted from the SH3–GK coupling to the structure of the PDZ3-C/SynGAP 15AA complex (PDB 5JXB). This analysis was done through comparison of the ^{1}H–^{15}N HSQC–TROSY spectra of PDZ3-C bound to SynGAP and that of P-S-G bound to SynGAP. The chemical shift difference of each peak is defined as $\Delta_{p.p.m.} = [(\Delta\delta_{HN})^2 + (\alpha N * \Delta\delta_{HN})^2]^{1/2}$. The scaling factor (αN) used to normalize the ^{1}H and ^{15}N chemical shift is 0.17. (e) Comparison of sequential backbone $d_{NN(i,\ i+1)}$ and $d_{NN(i,\ i+3)}$ nuclear Overhauser enhancement connectivity of PSD-95 αC before and after SynGAP 15AA peptide interaction. The extended part is highlighted with a green box. (f) Mapping of the backbone amide chemical shift changes of αC resulted from the SynGAP 15AA binding. The chemical shift difference of each peak is defined as $\Delta_{p.p.m.} = [(\Delta\delta_{HN})^2 + (\alpha N * \Delta\delta_{HN})^2]^{1/2}$. The scaling factor (αN) used to normalize the ^{1}H and ^{15}N chemical shift is 0.17. (g–h) AUC (G) and FPLC–SLS (H) analyses showing that binding of the CRIPT 17AA peptide cannot induce dimer/multimer formation of PSD-95 P-S-G. The same analyses also show that deletion of part of the αC in PDZ3-C (dEXT) also eliminates SynGAP binding-induced dimer/multimer formation of PSD-95 P-S-G.

broadenings to the SH3–GK part of the protein in the ^{14}N_PDZ–^{15}N_SH3GK/SynGAP complex. (Figs. 3b and S2C). Due to extensive signal broadening and peak overlaps of the SH3–GK part, we did not pursue chemical shift assignments for the peaks from the SH3–GK tandem.

P-S-G coupling is mediated by the extended helix of PDZ3

Comparison of the ^{1}H–^{15}N HSQC spectrum of ^{15}N_PDZ–^{14}N_SH3GK/SynGAP complex with that of ^{15}N-PDZ3-C/SynGAP (Figs. 3c and S3B) allowed

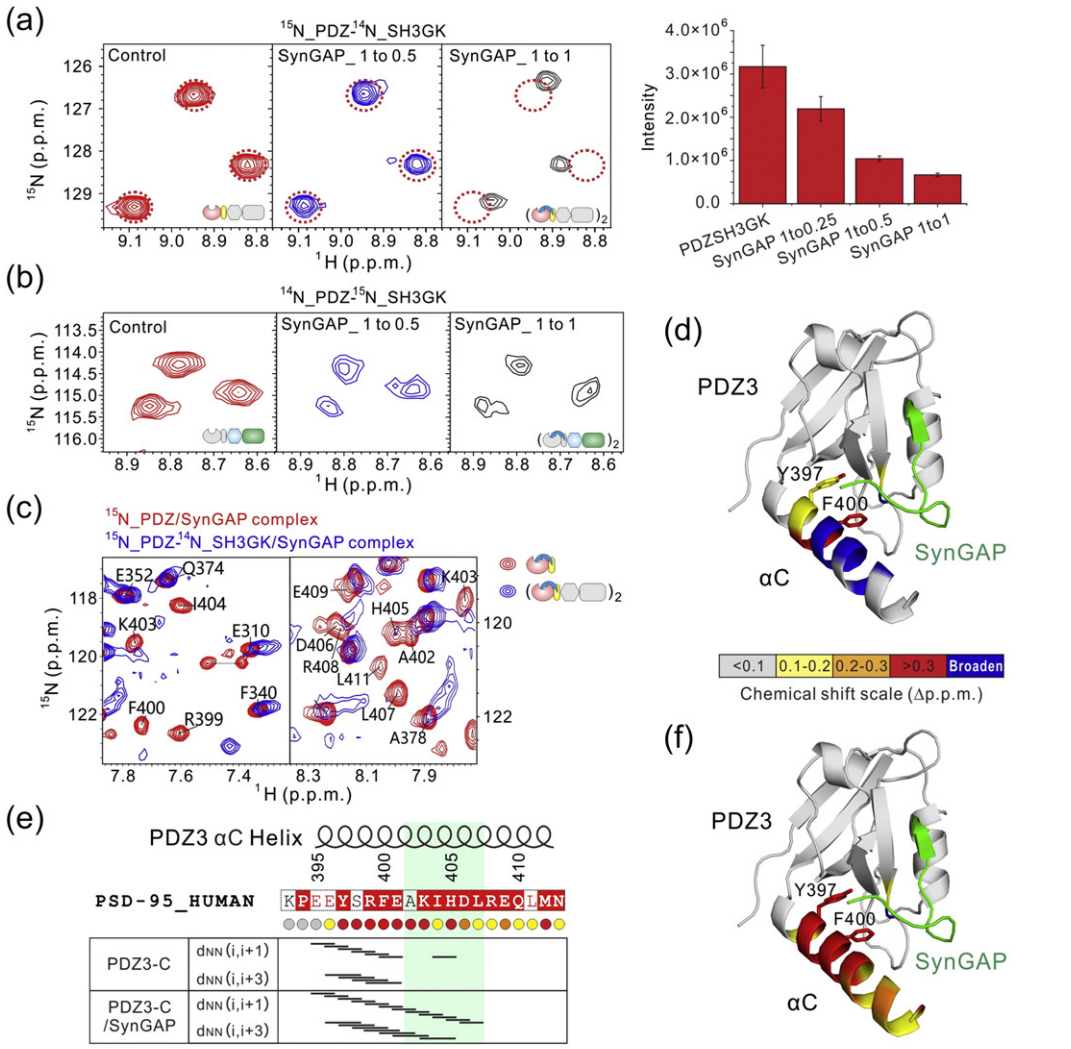

PSD-95 P-S-G	Theoretical MW (kDa)	AUC detected MW (kDa) with CRIPT	AUC detected MW (kDa) with SynGAP
WT	47.2	53.9	
dEXT	45.8		52.8

Fig. 3 (*legend on previous page*)

us to map the residues from PDZ3-C involved in the SynGAP binding-induced PDZ3-C/SH3–GK coupling of PSD-95 P-S-G. Multiple residues on PDZ3-C showed significant peak shifts or broadening (Fig. 3c and S3B), indicating that these residues are involved in the PDZ3-C/SH3–GK coupling. We mapped the residues experienced obvious chemical shift changes or peak broadenings onto the three-dimensional structure of PDZ3-C. The changing residues are predominantly located in the extended αC-helix of PDZ3 (Fig. 3d), indicating that this helical extension is responsible for coupling PDZ3 with SH3–GK when PSD-95 P-S-G binds to SynGAP. It is noted that two residues Y397 and F400 from the αC-helix, which directly interact with the SynGAP peptide but away from the SH3–GK tandem, experience large chemical shift changes upon PDZ3/SH3–GK coupling (Fig. 3d). This provides an explanation for why inclusion SH3–GK can enhance the SynGAP binding to PDZ3-C (Fig. 1f). Our NMR analysis also revealed that binding of the SynGAP peptide elongates and stabilizes αC-helix of PDZ3 (Fig. 3e, f and Fig. S3C, D). Earlier NMR studies of the apo PSD-95 P-S-G showed that the αC-helix is only partially formed (residues 394P-399R), and there is only minimal interaction between PDZ3-$C_{partial}$ with the SH3–GK unit ([38] and also see Fig. 2 in this study). It is envisioned that the SynGAP binding-induced PDZ3 αC-helix stabilization physically couples PDZ3-C with SH3–GK. We noted that the residues forming the PDZ3 αC-helix are highly conserved in all DLGs including the most primitive form of DLG from *choanoflagellata*, suggesting an ancient regulatory role of this helix.

We directly tested the role of αC-helix in ligand-induced PDZ3-C/SH3–GK coupling by deleting part of this helix from PSD-95 (deleting residues 402A-413N; see Fig. S3A for the sequence-specific backbone assignment of PDZ3-C/SynGAP 15AA and the mutant P-S-G is denoted as dEXT). The deletion of residues 402A-413N should eliminate the SynGAP binding-induced PDZ3 αC-helix elongation, but do not perturb PDZ3 folding and part of the αC-helix formation as reported in the literature [43]. Both AUC- and FPLC–SLS-based analyses showed that PSD-95 P-S-G dEXT adopts as a highly homogenous monomer in solution both with and without the presence of the saturated amount of SynGAP 15AA (Fig. 3g, h), indicating that the αC-helix of PDZ3-C is critical for mediating the conformational coupling between PDZ3-C and SH3–GK in PSD-95 P-S-G. We also investigated the binding of a synthetic peptide containing the last 17 residues of CRIPT, another PDZ3 binding ligand but does not induce PDZ3-C extension [44], to PSD-95 P-S-G. We could not detect any CRIPT peptide binding-induced PSD-95 P-S-G dimerization/multimerization even with the addition of 10 molar ratio amount of the CRIPT peptide (Fig. 3g, h). Therefore, the formation of the PSD-95 P-S-G multimer is specifically induced by the binding of SynGAP, which is a specific PSD-95 binding partner in synapses [40].

SynGAP-induced PDZ3-C/SH3–GK coupling in other DLG proteins

In the PSD, another two abundant DLG family members are PSD-93 and SAP102, sharing similar domain organizations with PSD-95 and are required for basal transmissions. We wondered whether SynGAP can also induce PDZ3-C/SH3–GK coupling in PSD-93 and SAP102. We first tested our hypothesis by analytical gel filtration chromatography. SynGAP 15AA-saturated PSD-93 PDZ3-C (residues 418E-523S) and PSD-93 SH3–GK (residues 530S-852L) mixture was eluted at an obviously smaller volume than the isolated PDZ3-C and SH3–GK mixture, indicating that SynGAP can induce direct coupling between PDZ3-C and SH3–GK of PSD-93 (Fig. 4a, left panel, blue curve *versus* pink curve). To our surprise, SAP102 PDZ3-C (residues 400R-506S), with or without the presence of SynGAP 15AA, does not interact with its own SH3–GK (residues 513S-849L) (Fig. 4a, right panel).

We verified the gel filtration chromatography results on the PDZ3-C to SH3–GK coupling of PSD-93 and SAP102 by AUC and FPLC–SLS. Very similar to what was observed for PSD-95, the apo-form of PSD-93 P-S-G (residues 418E-852L) adopts as a homogenous monomer in solution, and SynGAP binding induces dimer/multimer formation of the P-S-G tandem (Fig. 4b, c). The relatively broad AUC peak of the SynGAP peptide-bound PSD-93 P-S-G suggests that the multimeric forms of the ligand-bound P-S-G may undergo fast exchange in solution. In addition, we further showed by the ITC-based assay that, analogous to the PSD-95 P-S-G, direct coupling of PDZ3-C and SH3–GK can enhance SynGAP binding of PSD-93 P-S-G (Fig. 4d). In contrast, SAP102 P-S-G (residues 400R-849L) always adopts as a homogenous monomer in solution regardless the absence or presence of the SynGAP peptide (Fig. 4b, c). ITC-based binding assay showed that the SynGAP 15AA peptide binds to SAP102 PDZ3-C with a comparable affinity as it does to PSD-95 PDZ3-C (K_d ~3 μM for SAP102 *versus* ~4 μM for PSD-95; Figs. 1f and 4d), ruling out the possibility that non-observable PDZ3-C/SH3–GK coupling of SAP102 is because of lack of binding between SynGAP and SAP102. Consistent with the lack of direct coupling between PDZ3-C and SH3–GK observed in the hydrodynamic analyses, the SAP102 P-S-G tandem binds to the SynGAP peptide with the same affinity as its PDZ3-C does (Fig. 4d). Together, the above biochemical and biophysical studies reveal a surprising finding that the different

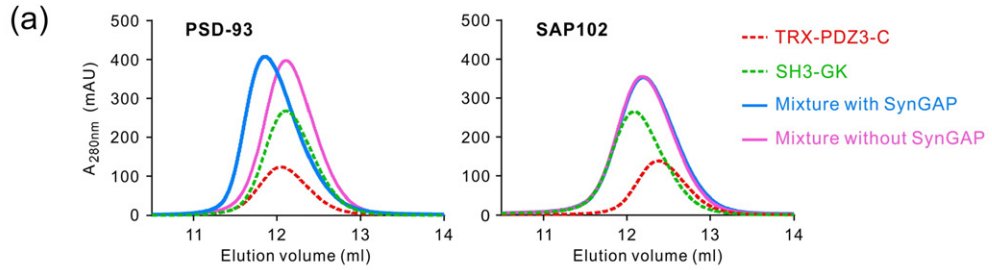

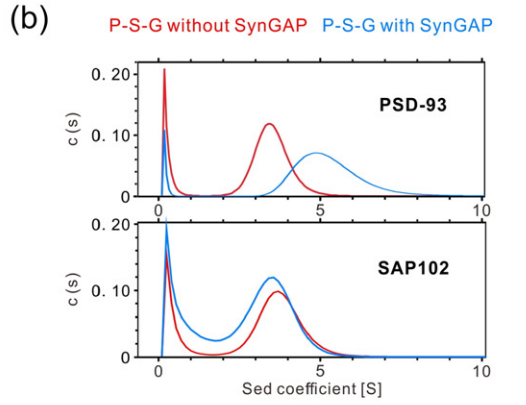

	Theoretical MW (kDa)	AUC detected MW (kDa)
PSD-93_P-S-G	48.9	51.9
PSD-93_P-S-G/SynGAP	50.7	99.7
SAP102_P-S-G	50.9	51.9
SAP102_P-S-G/SynGAP	52.7	52.5

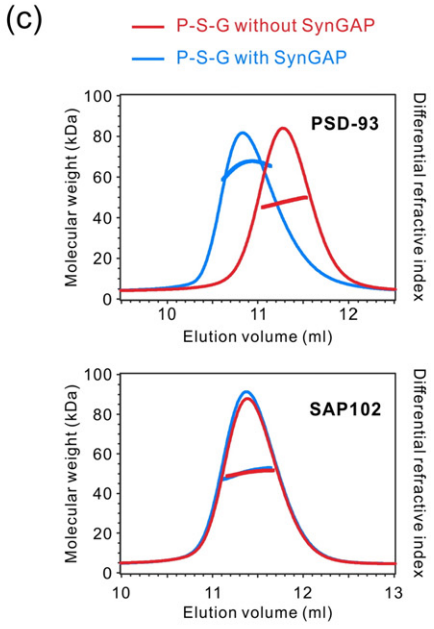

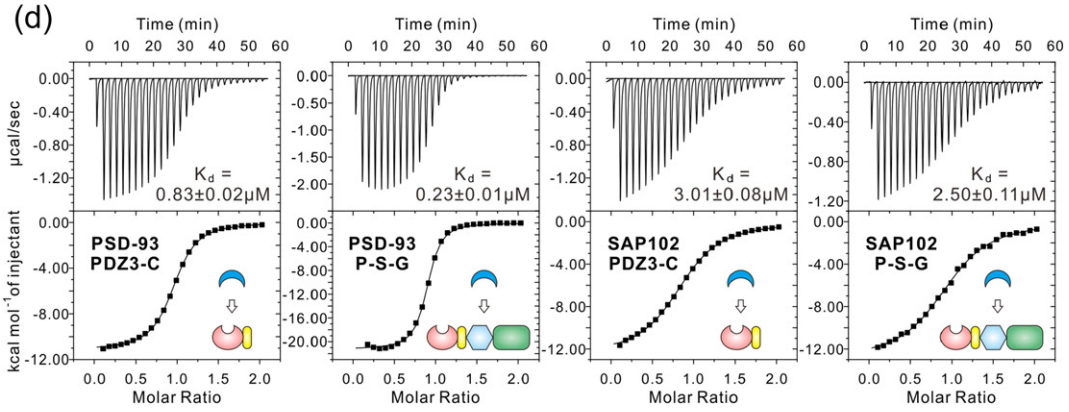

Fig. 4. SynGAP induces PSD-93, but not SAP102, PDZ3-C/SH3–GK coupling. (a) Analytical gel filtration chromatography showing that SynGAP 15AA induces direct binding between PSD-93 PDZ3-C and SH3–GK but not SAP102. The concentrations of proteins used in the experiments are 100 µM TRX-PDZ3-C, 100 µM SH3–GK-His, and 200 µM SynGAP 15AA peptide. (b) AUC analysis showing the SynGAP 15AA binding-induced PSD-93, but not SAP102, P-S-G dimerization/multimerization. The fitted molecular masses are presented in the table below the panel. (c) FPLC–SLS analysis showing that the SynGAP 15AA binding induces PSD-93 P-S-G molecular mass increase, but does not change the molecular mass of SAP102 P-S-G. The concentrations of proteins used in the experiments are 100 µM P-S-G with or without the presence of 200 µM SynGAP 15AA peptide. (d) ITC titration profiles showing that PSD-93 P-S-G has increased binding affinity to SynGAP 15AA than PDZ3-C alone does, whereas SAP102 P-S-G and PDZ3-C have no difference in binding to SynGAP 15AA. The titrations were performed by titrating 300 µM 15AA peptide into 30 µM PSD-93 (or SAP102) P-S-G or 400 µM 15AA peptide into 40 µM TRX-PDZ3-C of PSD-93 (or SAP102).

paralogs of DLGs have distinct differences in SynGAP binding-induced inter-domain conformational couplings and subsequent oligomerizations.

PDZ3-C/SH3–GK coupling specificities of DLGs are determined by their GK domains

Our NMR-based study revealed that the elongated PDZ3 C-terminal αC-helix is the major PDZ3-C/SH3–GK coupling site in PSD-95 (Fig. 3d). Sequence alignment shows that this region is extremely conserved among different DLG paralogs (Fig. 5a). Therefore, we hypothesized that the distinct PDZ3-C/SH3–GK coupling properties of DLG paralogs are likely determined by their SH3–GK instead of PDZ3-C.

We tested this hypothesis by mixing PDZ3-C from one DLG and SH3–GK from a different member and assayed interactions of such inter-DLG PDZ3-C/SH3–GK combinations by analytical gel filtration chromatography. In addition to interacting with its own PDZ3-C, PSD-95 SH3–GK also directly interacts with PSD-93 and SAP102 PDZ3-C domains when PDZ3-Cs are in complex with 15AA (Fig. 5b, above panels). In contrast, SAP102 SH3–GK interacts neither with PSD-95 PDZ3-C saturated with SynGAP 15AA nor with the PSD-93 PDZ3-C/15AA complex (Fig. 5b, below panels).

We further narrowed down the PDZ3-C/SH3–GK coupling determinant to the GK domain in DLGs. We made two chimeric DLG P-S-G proteins: one with the SAP102 PDZ3–SH3 fused with PSD-95 GK and the other with PSD-95 PDZ3–SH3 fused with SAP102 GK. Both chimeric proteins are well folded as indicated by their circular dichroism spectra (data not shown). Without SynGAP 15AA, both chimeric proteins are monomers in solution (Fig. 5c, d). After binding to SynGAP 15AA, the chimeric P-S-G containing the SAP102 GK failed to form SynGAP binding-induced dimerization (Fig. 5c, D1). The other chimera containing PSD-95 GK fused to SAP102 PDZ3–SH3 underwent SynGAP binding-induced dimerization (Fig. 5c, D2). The above data indicate that the GK domain plays a determinant role in the SynGAP-induced conformational coupling between PDZ3-C and SH3–GK in DLGs.

DLG hetero-dimer/oligomer formation

The results that different combinations of PDZ3-C and SH3–GK between DLG paralogs can interact with each other (Fig. 5b) immediately suggest that DLGs may form ligand-induced hetero-dimer/oligomers. We used DSG-mediated crosslinking experiments to probe this hypothesis. We fused a GB1-tag (~8.0 kDa) to the C-terminus of PSD-93 P-S-G (referred to as 93_P-S-G-GB1) so that the three DLG P-S-G tandems can be clearly differentiated on SDS-PAGE gel (Fig. 5E1, lanes 1–3). First, SynGAP-mediated PSD-95 and PSD-93 P-S-G homo-dimer/oligomer can be captured by DSG-mediated crosslinking (Fig. 5E1, lanes 1/4/7 and lanes 2/5/8). SynGAP 15AA does not induce SAP102 homo-dimer formation (Fig. 5E1, lanes 3/6/9). The faint high-molecular-mass bands in *lane 9* are likely non-specific as similar faint bands were also observed in SAP102/DSG group without adding 15AA (Fig. 5E1, lanes 9 *versus* lane 6). In the mixtures of PSD-95 P-S-G/PSD-93 P-S-G-GB1/15AA and PSD-95 P-S-G/SAP102 P-S-G/15AA (both at the 1:1:5 molar ratio to ensure that the P-S-G tandems are saturated by the SynGAP peptide), DSG crosslinking captured P-S-G hereto-dimers/oligomers in addition to the homo-dimers/oligomers in each reaction (Fig. 5E1, lanes 7–11 and zoomed-in in Fig. 5E2). For example, we tentatively assigned the bands with molecular masses between PSD-95 P-S-G homo-dimer and PSD-93 P-S-G-GB1 homo-dimer in lane 10 as hetero-dimers formed by PSD-95 P-S-G and PSD-93 P-S-G-GB1 hetero-dimer simply based on the molecular weight calculations (Fig. 5E2). It should be noted that such assignment is tentative, and additional experiments would be required to define the nature of these crosslinked bands.

Ligand-induced PDZ/SH3–GK coupling in other MAGUKs

Since all MAGUKs, except for MAGIs, contain a P-S-G tandem in their domain organizations, we asked whether that ligand-induced PDZ/SH3–GK coupling observed for DLGs may also occur in other MAGUKs. We tested this hypothesis by investigating P-S-G tandems from PALS1 and CASK. PALS1 is crucial for cell polarity determination by forming the PALS1/Crumbs/PATJ complex acting as a master cell growth and polarity regulator in apical membranes of polarized epithelial cells [45]. CASK is a MAGUK protein playing essential roles in the presynaptic terminus, anchoring presynaptic adhesion molecule Neurexin [46]. We chose these two MAGUKs because the PDZ ligands for each of the two P-S-G tandems are well defined and earlier characterized by our lab [35].

To monitor possible PDZ/SH3–GK couplings of the two MAGUK P-S-G tandems by NMR spectroscopy, we selectively labeled the PDZ domains of PALS1 and CASK P-S-G with ^{15}N using the sortase-based protein ligation method shown in Fig. 2. The PALS1 and CASK P-S-G tandems derived from the sortase ligation method (referred to as P-$_{LPETGG}$-SG) displayed the essentially same target binding affinities when compared to their respective native P-S-G tandems (Fig. 6a, b). In addition, we further verified that the P-S-G tandems of PALS1 and CASK bind to their respective PDZ

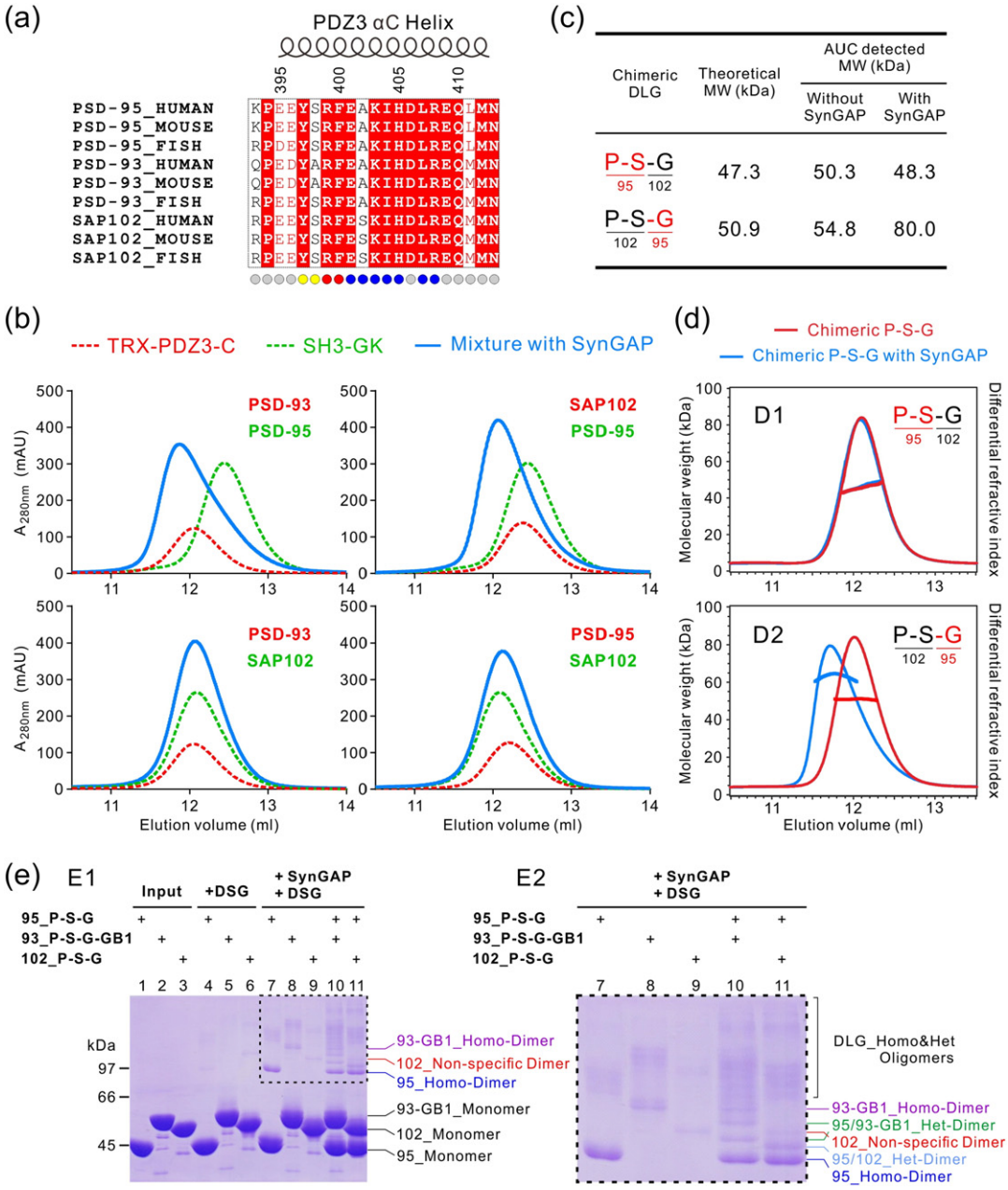

Fig. 5. The GK domain determines the coupling specificity between PDZ3-C and SH3–GK of DLG paralogs. (a) Sequence alignment of DLGs PDZ3 C-terminal αC-helix showing that this region is highly conserved during evolution. The color of the circle below each residue is consistent with the residue color in Fig. 3d. (b) Analytical gel filtration chromatography showing that PSD-95 SH3–GK interacts with PSD-93 PDZ3-C/15AA or with SAP102 PDZ3-C/15AA, while SAP102 SH3–GK does not interact with PSD-95 PDZ3-C/15AA or with PSD-93 PDZ3-C/15AA. The concentrations of proteins used in the experiments are: 100 μM TRX-PDZ3-C, 100 μM SH3–GK-His, 200 μM SynGAP 15AA peptide. (c) Summery of AUC-derived molar masses of the two chimeric DLG P-S-G proteins without or with two molar ratios of SynGAP 15AA. (d) FPLC–SLS analysis showing that the chimeric DLG P-S-G with the PSD-95 GK replaced by SAP102 GK failed to form SynGAP 15AA binding-induced multimerization (D1). In contrast, another DLG P-S-G chimera with the SAP102 GK replaced by PSD-95 GK gained SynGAP 15AA binding-induced multimerization (D2). The concentrations of proteins used in the experiments are 100 μM chimeric P-S-G with or without the presence of 200 μM SynGAP 15AA peptide. (e) DSG-mediated crosslinking reveals that DLGs undergo SynGAP 15AA-induced homo- or hetero-dimerization/multimerization. The dashed box in the left panel is enlarged at the right for easy viewing of the crosslinked, multimeric forms of homo- and hetero-DLG oligomers.

ligands (the Crumbs tail and the Neurexin tail, respectively) with much higher affinities than their isolated PDZ domains (Fig. 6b) [35].

NMR-based titration experiments using the selective ^{15}N-labeled P-S-G samples were used to test whether the P-S-G tandems of these two MAGUKs

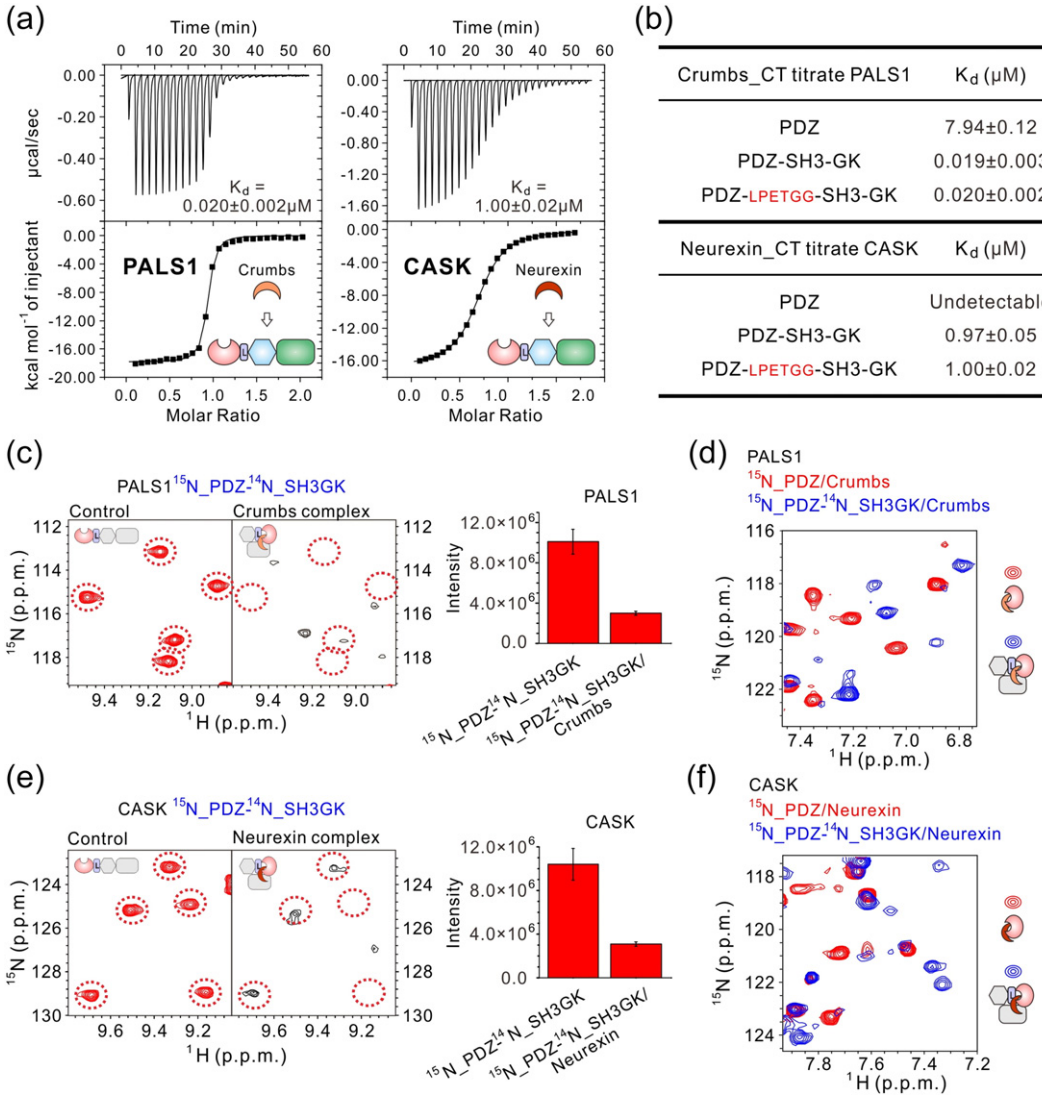

Fig. 6. Ligand-induced PDZ/SH3–GK coupling of the PALS1 and CASK P-S-G tandems. (a–b) ITC titration profiles showing that the PALS1 and CASK P-S-G tandems prepared by the sortase-ligation method display same ligand binding properties to their respective native proteins. In addition, both PALS1 and CASK P-S-G tandems bind to their respective ligands with significantly higher affinity than their isolated PDZ domains. The ITC titration experiments were performed by titrating 300 or 100 μM Crumbs 22AA peptide to 30 μM PALS1 TRX-PDZ or 10 μM P-S-G, respectively, in the cell, or 500 or 300 μM Neurexin 22AA peptide to 50 μM CASK TRX-PDZ or 30 μM P-S-G, respectively, in the cell. (c) A selected region of the ^{1}H,^{15}N HSQC–TROSY spectra of the apo- or Crumbs peptide-saturated PALS1 ^{15}N_PDZ–^{14}N_SH3GK (referred to Fig. S4B for the full spectra). The average peak intensity of the residues from the PDZ domain before and after the Crumbs 22AA binding is quantified and presented using the bar diagram at right. (d) Superposition plot of a selected region of ^{1}H,^{15}N HSQC–TROSY spectra of PALS1 ^{15}N-PDZ in saturated with Crumbs 22AA (red peaks) and of PALS1 ^{15}N_PDZ–^{14}N_SH3GK saturated with Crumbs 22AA (blue peaks), showing obvious SH3–GK coupling-induced spectral changes to the PDZ domain of PALS1 P-S-G. The full spectra are shown in Fig. S4C. (e) A selected region of the ^{1}H,^{15}N HSQC–TROSY spectra of the apo- or Neurexin peptide-saturated CASK ^{15}N_PDZ–^{14}N_SH3GK (referred to Fig. S5B for the full spectra). The average peak intensity of the residues from the PDZ domain before and after the Neurexin 22AA binding is quantified and presented using the bar diagram at right. (f) Superposition plot of two selected regions of ^{1}H,^{15}N HSQC–TROSY spectra of CASK ^{15}N–PDZ-C in saturated with the Neurexin 22AA (red peaks) and of ^{15}N_PDZ–^{14}N_SH3GK saturated with the Neurexin 22AA (blue peaks). Again, obvious SH3–GK coupling-induced spectral changes to the PDZ domain of CASK P-S-G are observed. The full spectra are shown in Fig. S5C.

also undergo ligand binding-induced PDZ/SH3–GK couplings. First, we observed very little direct coupling between PDZ and SH3–GK of both MAGUKs in their apo-forms, and the peak intensity of the PDZ domains alone or in the P-S-G tandems is comparable (Figs. S4A and S5A). Addition of one molar ratio of the Crumbs C-terminal peptide (the last 22 residues of human Crumbs1, referred to as Crumbs-CT) into PALS1 ^{15}N_PDZ–^{14}N_SH3GK leads to overall chemical shift changes as well as significant peak intensity decreases to the ^{15}N-labeled PDZ domain (Figs. 6c and S4B), similar to what was observed in the PSD-95 P-S-G/SynGAP interaction (Fig. 3). As the control, Crumbs-CT binding to the isolated PDZ domain of PALS1 induced marginal peak broadening (Fig. S4D). The dramatic Crumbs-CT binding-induced signal broadening suggests that PALS1 P-S-G also undergoes Crumbs binding-induced PDZ/SH3–GK coupling. A number of residues in the PALS1 PDZ experience chemical shift changes upon SH3–GK coupling (Figs. 6d and S4C), and these residues are presumably involved in the PDZ/SH3–GK coupling in PALS1 P-S-G. Using the same strategy, we found that Neurexin C-terminal (the last 22 residues of mouse Neurexin1, referred to as Neurexin-CT) binding to the selectively ^{15}N-labeled CASK P-S-G (^{15}N_PDZ–^{14}N_SH3GK) also caused significant peak broadening as well as chemical shift changes to the PDZ domain (Figs. 6e and S5B). A set of residues on the PDZ domain similarly showed SH3–GK coupling-induced chemical shift changes (Figs. 6f and S5C), and these residues may be involved in the PDZ/SH3–GK coupling in CASK P-S-G. In summary, our NMR-based studies reveal that PDZ ligand binding-induced PDZ/SH3–GK couplings also occur in the P-S-G tandems of PALS1 and CASK.

Discussion

PDZ ligand binding-induced PDZ/SH3–GK coupling and the P-S-G supramodule formation of MAGUKs

The common P-S-G tandem domain organization of MAGUKs hints that the three domains in P-S-G tandems may cooperate with each other forming higher order structures with unique cellular functions. Several previous studies have shown that, when bound to target proteins, the P-S-G tandems from several MAGUKs including PALS1 and ZO-1 indeed form integral structural suprmodules [35–37]. However, it is not known whether these P-S-G supramodule formations also occur in the apo-form proteins. In addition, whether the DLG family P-S-G tandems form stable supramodule is debatable, although earlier studies have suggested that PDZ3 can transiently interact with SH3–GK in the apo-form of PSD-95 P-S-G [38,39]. Here we report that the structural couplings between PDZ3 and SH3–GK in the apo-form of DLG MAGUKs are minimal. We found that binding of SynGAP to the PSD-95 PDZ3-C induces structural coupling between PDZ3-C and SH3–GK. Using segmentally ^{15}N-labeled PSD-95 P-S-G samples, we have been able to elucidate the molecular mechanism governing the SynGAP binding-induced conformational coupling between PDZ3-C and SH3–GK of PSD-95. We found that the binding of SynGAP elongates and stabilizes the αC-helix immediately following the C-terminal end of the canonical PDZ3 fold (Fig. 3e, f and Fig. S3C, D), and this extended α-helix is responsible for directly coupling to SH3–GK of the P-S-G tandem. The formation of the P-S-G supramodule, in return, further enhances SynGAP binding of PSD-95. The conformational restraints of the linker connecting PDZ3-C and SH3 in PSD-95 P-S-G induced by the SynGAP binding (i.e., the shortened flexible linker due to the PDZ3-C αC-helix elongation) may have forced the domain-swapped P-S-G dimer or multimer formation (Fig. 7), as insertion of a stretch of flexible residues into the linker between the PDZ3 αC-helix and the SH3 domain essentially eliminated the SynGAP binding-induced P-S-G dimer formation (Fig. S6). We further discovered that PSD-93 P-S-G behaves essentially the same as PSD-95 P-S-G does in undergoing SynGAP binding-induced PDZ3-C/SH3–GK coupling and P-S-G multimerization. Surprisingly, SAP102 P-S-G does not undergo SynGAP binding-induced supramodule formation and multimerization. We found that the GK domain of each paralog of DLGs determines whether their P-S-G tandems can undergo PDZ ligand binding-induced conformational couplings. Finally, we demonstrate using the segmental ^{15}N-labeling approach combined with NMR spectroscopy that the P-S-G tandems from two other MAGUKs (PALS1 and CASK) can also undergo specific PDZ ligand binding-induced PDZ/SH3–GK coupling. Therefore, we believe that the PDZ ligand binding-induced PDZ/SH3–GK coupling is a rather common mechanism used by MAGUKs in general. Our findings also provide a possible explanation for why the P-S-G tandem organization is highly conserved in the MAGUK family scaffold proteins, as the P-S-G supramodules of the MAGUKs are likely positively selected by both their structural and functional roles during the evolution.

DLG multimerization and PSD organization

DLGs (PSD-95, PSD-93, and SAP102) are key structural organizers of the PSD. In addition, DLGs are critical for anchoring and organizing both

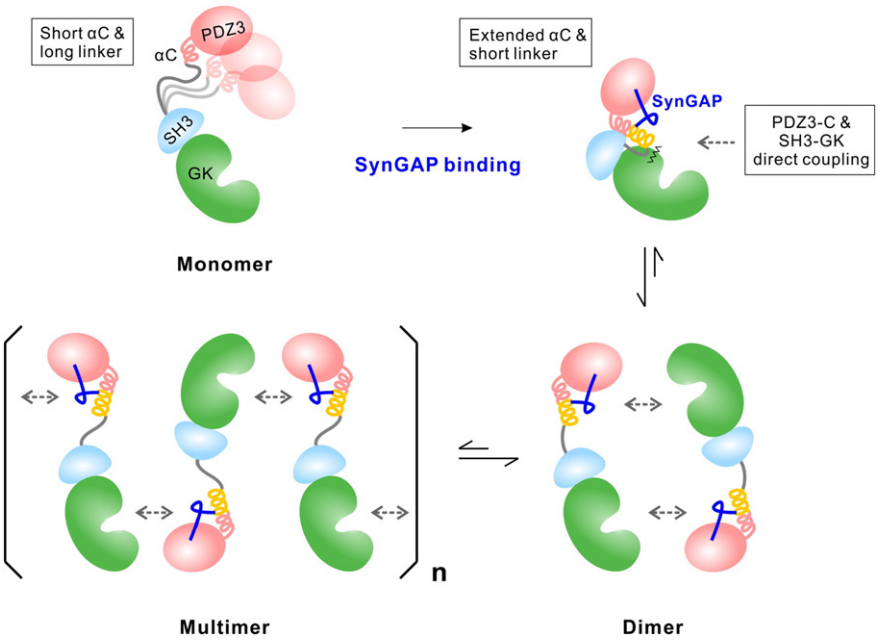

Fig. 7. Model of SynGAP binding-induced PSD-95 P-S-G conformational coupling. Without SynGAP binding, the linker between PSD-95 PDZ3 and SH3 is flexible. SynGAP binding elongates and stabilizes PDZ3-C αC-helix, which further promotes PDZ3-C/SH3–GK coupling. SynGAP binding also triggers PSD-95 P-S-G dimerization and multimerization due to the ligand binding-induced shortening of the PDZ3–SH3 linker and the resulting potential intra-molecular conformational restraints.

NMDAR and AMPAR signaling complexes at the postsynaptic membranes [25,26]. Extensive studies in the past have revealed that different members of DLGs can cooperate with each other in dictating PSD structural organization and synaptic transmissions [23,25]. There are also biochemical evidences showing that different DLG paralogs can stabilize each other in synapses *in vivo* [32]. As one would expect, each DLG paralog must have its unique physiological functions [7,47,48]. An attractive molecular model in connecting different signaling complexes organized by DLG paralogs is via the formation of DLG hetero-dimers/oligomers. However, whether DLGs can form homo- or even hetero-oligomers is largely unknown prior to this study, largely due to the lack of proper methods to investigate such questions. In this study, we demonstrated that, in addition to forming homo-oligomers, P-S-G tandems of DLGs can also form hetero-oligomers mediated by inter-molecular PDZ3-C/SH3–GK couplings. It is important to note that both homo- and hetero-oligomers of DLG P-S-G tandems are only formed upon specific target binding to the PDZ3 domain, suggesting that the DLG-organized mega PSD protein assembly formation can be modulated by synaptic activity-dependent protein enrichments or dispersions of DLG binding proteins such as SynGAP [40,49].

Our finding that PSD-95 and PSD-93, but not SAP102, can undergo SynGAP binding-induced dimer/multimer formation correlates well with observations from earlier studies of these DLG paralogs in the PSD. Using fluorescence recovery after photobleaching assay, it was reported that SAP102 is more mobile and diffuses deeper toward dendritic shafts than PSD-95 in synapses [50], correlating well with the lack of multimerization capacity of SAP102's P-S-G tandem. A more recent study employed biochemical and mouse genetic approaches to characterize the supermolecular PSD protein complex formation *in vivo*. They revealed that in mouse brain, NMDA receptors are partitioned into supramolecular complexes with a molar mass up to ~1.5 MDa [32]. Interestingly, both PSD-95 and PSD-93 are core components of this 1.5-MDa supracomplex and exist at a near stoichiometric ratio with the receptor. Knockout either PSD-95 or PSD-93 depletes the formation of almost all of 1.5-MDa NMDAR-DLG supracomplexes, suggesting that an association between and mutual stabilization of PSD-95 and PSD-93 is essential for the NMDAR receptor complex assembly. Our finding of the formation of the PSD-95/PSD-93 hetero-multimer formation provides an explanation for the PSD-95/PSD-93/NMDAR supramolecular complex organization observed in synapses *in vivo*.

Methods

Plasmids, peptides, protein expression, and purification

	Species	Full-length protein	Reference sequence
PSD-95	Human	724aa	NP_001308004
PSD-93	Rat	852aa	NP_071618
SAP102	Rat	849aa	NP_113827
PALS1	Human	675aa	NP_071919
CASK	Rat	909aa	NP_071520

	TRX-His_6-PDZ3-C	SH3–GK-His_6	PDZ3–SH3–GK
PSD-95	309R-415S-LPETGG	GG-422S-724L	309R-724L
PSD-93	418E-523S-LPETGG	GG-530S-852L	418E-852L
SAP102	400R-506S-LPETGG	GG-513S-849L	400R-849L
PSD-95 P-S-G dEXT			309R-724L Δ402A-413N
Chimeric 95_P-S-102_G			95_309R-V531 fuse 102_657H-849L
Chimeric 102_P-S-95_G			102_400R-656I fuse 95_532H-724L
PSD-95 $P_{\text{-23loop}}$-S-G			309R-422S-$_{(248N\text{-}308P)}$-423L-724L
PSD-95 $P_{\text{-6GGS}}$-S-G			309R-422S-$_{(6GGS)}$-423 L-724L

	TRX-His_6-PDZ	SH3–GK-His_6	P-S-G
PALS1	252E-338I-LPETGG	GGS-346T-675R	252E-675R
CASK	486 T-581D-LPETGG	GG-589S-909Y	486 T-909Y

Synthesized peptide names	Synthesized peptide sequences
SynGAP 15AA	AQRGSFPPWVQQTRV
CRIPT 17AA	MCGKKVLDTKNYKQTSV
Crumbs 22AA	EKEGSRVEMWNLMPPPAMERLI
Neurexin 22AA	KQPSSAKSANKNKKNKDKEYYV

Various fragments and mutants of MAGUKs are generated using standard PCR-based methods and confirmed by DNA sequencing. His-tagged sortase Δ59 plasmid is a kind gift from Prof. Xuewu Zhang in UT Southwestern Medical Center [51]. Proteins were expressed in *Escherichia coli* BL21 CondonPlus cells in LB medium at 16 °C and purified using a combination of nickel-NTA agarose, Mono Q column, and size-exclusion chromatography as see fit. Purified proteins were prepared in a buffer containing 50 mM Tris (pH 8.0), 100 mM NaCl, 1 mM EDTA, and 2 mM DTT for most characterizations. When needed, tags were cleaved by HRV 3C protease and separated by another step of size-exclusion chromatography. Uniformly ^{15}N, ^{13}C-labeled proteins were prepared by growing bacteria in M9 minimal medium supplemented with $^{15}NH_4Cl$ and ^{13}C-glucose. Peptides were commercially synthesized.

Sortase-mediated protein ligation

Protein ligations of the N-terminal TRX-His_6-tagged and C-terminal LPETGG-tagged MAGUK PDZ with the N-terminal GG-tagged and C-terminal His_6-tagged MAGUK SH3–GK were catalyzed by sortase Δ59. The reaction mixture contains PDZ, SH3–GK, and sortase Δ59 with 200, 100, and 50 μM, respectively, in buffer containing 50 mM Tris (pH 8.0), 100 mM NaCl, 1 mM EDTA, and 2 mM DTT. The reaction was triggered by adding 10 mM $CaCl_2$ and stopped by adding excess amount of EDTA. Each ligation reaction was carried in room temperature for about 1–1.5 h. The ligated TRX-P-S-G-His products were separated from unreacted reactants and the sortase by passing the reaction mixtures through a Superdex-75 gel filtration column. The N-terminal TRX-tag was then cleaved by HRV 3C protease and separated by another step of size-exclusion chromatography.

ITC assay

ITC measurements were carried out on a Microcal VP-ITC calorimeter at 25 °C. Proteins used for ITC measurements were dissolved in an assay buffer containing 50 mM Tris (pH 8.0), 100 mM NaCl, 1 mM

EDTA, and 2 mM DTT. High concentration of proteins was individually loaded into the syringe and titrated into the cell containing low concentration of corresponding interactors (protein concentrations for each specific reaction is specified in the corresponding figure legends). For each titration point, a 10-μL aliquot of a protein sample in the syringe was injected into the interacting protein in the cell at a time interval of 2 min. Titration data were analyzed using the Origin7.0 software and fitted with the one-site binding model.

NMR experiments

NMR samples contained 0.2 mM of PSD-95 P-S-G in 50 mM sodium phosphate (pH 8.0, with 2 mM DTT and 1 mM EDTA) in 90% H_2O/10% D_2O. transverse relaxation optimized spectroscopy (TROSY)–HSQC spectrum were acquired at 30 °C on Varian Inova 800-MHz spectrometers equipped with an actively z-gradient shielded triple resonance probe. Backbone resonance assignment of PSD-95 PDZ3-C and PSD-95 PDZ3-C in complex with unlabeled SynGAP 15AA were obtained using ^{15}N, ^{13}C-uniformly labeled PDZ3-C at a sample concentration ~1.2 mM dissolved in 50 mM sodium phosphate (pH 6.5 with 1 mM DTT and 1 mM EDTA). Standard heteronuclear triple resonance correlation experiments were recorded at 30 °C. Spectra were analyzed by using NMRPipe [52] and Sparky (T.D. Goddard and D.G. Kneller, SPARKY 3, University of California, San Francisco).

FPLC–SLS

The PDZ3-C to SH3–GK coupling analysis was performed on an AKTA FPLC system (GE Healthcare). P-S-G molar mass measurements were performed on an AKTA FPLC system coupled with an SLS detector (miniDAWN, Wyatt) and a differential refractive index detector (Optilab, Wyatt). Protein samples were loaded to a Superose 12 10/300 GL column pre-equilibrated by a column buffer composed of 50 mM Tris (pH 8.0), 100 mM NaCl, 1 mM EDTA, and 2 mM DTT. Data were analyzed with ASTRA6 (Wyatt). Protein concentrations in each reaction were illustrated in the corresponding figure legends.

AUC analysis

Sedimentation velocity experiments were performed on a Beckman XL-I analytical ultracentrifuge equipped with an eight-cell rotor at the speed of 33,000 rpm at 25 °C. The partial specific volume of protein samples and the buffer density were calculated using the program SEDNTERP[‡]. The final sedimentation velocity data were analyzed and fitted to a continuous sedimentation coefficient distribution model using the program SEDFIT[§]

Chemical crosslinking assay

DLG P-S-G (with affinity tags removed) and SynGAP 15AA peptide were prepared in buffer with 50 mM phosphate-buffered saline (pH 7.4), 100 mM NaCl, and 2 mM DTT. The DSG to protein ratio was set at 20:1 (10:1 in hetero-DLG crosslinking experiments), and the 15AA to DLG P-S-G ratio was set at 5:1 (2.5:1 in hetero-DLG crosslinking experiments). The reaction was carried out at room temperature for 20 min and quenched by 200 mM Tris (pH 8.3). Crosslinking products were analyzed by 10% SDS-PAGE with Coomassie blue staining.

Acknowledgments

This work in M.Z.'s lab has been supported by grants from RGC of Hong Kong (664113, 16103614, 16149516, and AoE-M09-12), a 973 program grant from the Minister of Science and Technology of China (2014CB910204), and a grant from the Asia Fund for Cancer Research. M.Z. is a Kerry Holdings Professor in Science and a Senior Fellow of IAS at HKUST.

Received 1 September 2017;
Received in revised form 20 October 2017;
Accepted 8 November 2017
Available online 11 November 2017

Keywords:
postsynaptic density;
synaptic signaling;
PSD-95;
MAGUK;
PDZ

†These authors contributed equally to the work.
‡http://www.rasmb.bbri.org/
§http://www.analyticalultracentrifugation.com/default.htm

Abbreviations used:
MAGUK, membrane-associated guanylate kinase; DLG, Discs large; PSD, postsynaptic density; SAP, synapse-associated proteins; NMDA, *N*-methyl-D-aspartate; AMPA, α-amino-3-hydroxy-5-methyl-4-isoxazolepropionic acid;

CASK, calcium/calmodulin-dependent serine protein kinase; PALS1, protein associated with Lin-7 1; ITC, isothermal titration calorimetry; AUC, analytical ultracentrifugation; FPLC, fast protein liquid chromatography; SLS, static light scattering.

References

[1] E.G. Gray, Axo-somatic and axo-dendritic synapses of the cerebral cortex: an electron microscope study, J. Anat. 93 (1959) 420–433.

[2] W. Feng, M. Zhang, Organization and dynamics of PDZ-domain-related supramodules in the postsynaptic density, Nat. Rev. Neurosci. 10 (2009) 87–99.

[3] M.S. Lowenthal, S.P. Markey, A. Dosemeci, Quantitative mass spectrometry measurements reveal stoichiometry of principal postsynaptic density proteins, J. Proteome Res. 14 (2015) 2528–2538.

[4] M. Sheng, C.C. Hoogenraad, The postsynaptic architecture of excitatory synapses: a more quantitative view, Annu. Rev. Biochem. 76 (2007) 823–847.

[5] J. Zhu, Y. Shang, M. Zhang, Mechanistic basis of MAGUK-organized complexes in synaptic development and signalling, Nat. Rev. Neurosci. 17 (2016) 209–223.

[6] C. Oliva, P. Escobedo, C. Astorga, C. Molina, J. Sierralta, Role of the MAGUK protein family in synapse formation and function, Dev. Neurobiol. 72 (2012) 57–72.

[7] S. Won, J.M. Levy, R.A. Nicoll, K.W. Roche, MAGUKs: multifaceted synaptic organizers, Curr. Opin. Neurobiol. 43 (2017) 94–101.

[8] L. Funke, S. Dakoji, D.S. Bredt, Membrane-associated guanylate kinases regulate adhesion and plasticity at cell junctions, Annu. Rev. Biochem. 74 (2005) 219–245.

[9] B.M. Muller, U. Kistner, R.W. Veh, C. Cases-Langhoff, B. Becker, E.D. Gundelfinger, et al., Molecular characterization and spatial distribution of SAP97, a novel presynaptic protein homologous to SAP90 and the *Drosophila* discs-large tumor suppressor protein, J. Neurosci. 15 (1995) 2354–2366.

[10] J.E. Brenman, K.S. Christopherson, S.E. Craven, A.W. McGee, D.S. Bredt, Cloning and characterization of post-synaptic density 93, a nitric oxide synthase interacting protein, J. Neurosci. 16 (1996) 7407–7415.

[11] E. Kim, K.O. Cho, A. Rothschild, M. Sheng, Heteromultimerization and NMDA receptor-clustering activity of Chapsyn-110, a member of the PSD-95 family of proteins, Neuron 17 (1996) 103–113.

[12] B.M. Muller, U. Kistner, S. Kindler, W.J. Chung, S. Kuhlendahl, S.D. Fenster, et al., SAP102, a novel postsynaptic protein that interacts with NMDA receptor complexes in vivo, Neuron 17 (1996) 255–265.

[13] K.O. Cho, C.A. Hunt, M.B. Kennedy, The rat brain postsynaptic density fraction contains a homolog of the *Drosophila* discs-large tumor suppressor protein, Neuron 9 (1992) 929–942.

[14] U. Kistner, B.M. Wenzel, R.W. Veh, C. Cases-Langhoff, A.M. Garner, U. Appeltauer, et al., SAP90, a rat presynaptic protein related to the product of the *Drosophila* tumor suppressor gene dlg-A, J. Biol. Chem. 268 (1993) 4580–4583.

[15] L. Chen, D.M. Chetkovich, R.S. Petralia, N.T. Sweeney, Y. Kawasaki, R.J. Wenthold, et al., Stargazin regulates synaptic targeting of AMPA receptors by two distinct mechanisms, Nature 408 (2000) 936–943.

[16] S. Dakoji, S. Tomita, S. Karimzadegan, R.A. Nicoll, D.S. Bredt, Interaction of transmembrane AMPA receptor regulatory proteins with multiple membrane associated guanylate kinases, Neuropharmacology 45 (2003) 849–856.

[17] H.C. Kornau, L.T. Schenker, M.B. Kennedy, P.H. Seeburg, Domain interaction between NMDA receptor subunits and the postsynaptic density protein PSD-95, Science 269 (1995) 1737–1740.

[18] A.S. Leonard, M.A. Davare, M.C. Horne, C.C. Garner, J.W. Hell, SAP97 is associated with the alpha-amino-3-hydroxy-5-methylisoxazole-4-propionic acid receptor GluR1 subunit, J. Biol. Chem. 273 (1998) 19518–19524.

[19] E. Schnell, M. Sizemore, S. Karimzadegan, L. Chen, D.S. Bredt, R.A. Nicoll, Direct interactions between PSD-95 and stargazin control synaptic AMPA receptor number, Proc. Natl. Acad. Sci. U. S. A. 99 (2002) 13902–13907.

[20] A.W. McGee, S.R. Dakoji, O. Olsen, D.S. Bredt, W.A. Lim, K.E. Prehoda, Structure of the SH3-guanylate kinase module from PSD-95 suggests a mechanism for regulated assembly of MAGUK scaffolding proteins, Mol. Cell 8 (2001) 1291–1301.

[21] G.A. Tavares, E.H. Panepucci, A.T. Brunger, Structural characterization of the intramolecular interaction between the SH3 and guanylate kinase domains of PSD-95, Mol. Cell 8 (2001) 1313–1325.

[22] J. Zhu, Y. Shang, C. Xia, W. Wang, W. Wen, M. Zhang, Guanylate kinase domains of the MAGUK family scaffold proteins as specific phospho-protein-binding modules, EMBO J. 30 (2011) 4986–4997.

[23] G.M. Elias, L. Funke, V. Stein, S.G. Grant, D.S. Bredt, R.A. Nicoll, Synapse-specific and developmentally regulated targeting of AMPA receptors by a family of MAGUK scaffolding proteins, Neuron 52 (2006) 307–320.

[24] M. Migaud, P. Charlesworth, M. Dempster, L.C. Webster, A.M. Watabe, M. Makhinson, et al., Enhanced long-term potentiation and impaired learning in mice with mutant postsynaptic density-95 protein, Nature 396 (1998) 433–439.

[25] J.M. Levy, X. Chen, T.S. Reese, R.A. Nicoll, Synaptic consolidation normalizes AMPAR quantal size following MAGUK loss, Neuron 87 (2015) 534–548.

[26] X. Chen, J.M. Levy, A. Hou, C. Winters, R. Azzam, A.A. Sousa, et al., PSD-95 family MAGUKs are essential for anchoring AMPA and NMDA receptor complexes at the postsynaptic density, Proc. Natl. Acad. Sci. U. S. A. 112 (2015) E6983–92.

[27] S.E. Craven, A.E. El-Husseini, D.S. Bredt, Synaptic targeting of the postsynaptic density protein PSD-95 mediated by lipid and protein motifs, Neuron 22 (1999) 497–509.

[28] D. El-Husseini Ael, E. Schnell, S. Dakoji, N. Sweeney, Q. Zhou, O. Prange, et al., Synaptic strength regulated by palmitate cycling on PSD-95, Cell 108 (2002) 849–863.

[29] W. Feng, J.F. Long, J.S. Fan, T. Suetake, M. Zhang, The tetrameric L27 domain complex as an organization platform for supramolecular assemblies, Nat. Struct. Mol. Biol. 11 (2004) 475–480.

[30] W. Feng, J.F. Long, M. Zhang, A unified assembly mode revealed by the structures of tetrameric L27 domain complexes formed by mLin-2/mLin-7 and Patj/Pals1 scaffold proteins, Proc. Natl. Acad. Sci. U. S. A. 102 (2005) 6861–6866.

[31] J. Nithianantharajah, N.H. Komiyama, A. McKechanie, M. Johnstone, D.H. Blackwood, D. St Clair, et al., Synaptic

scaffold evolution generated components of vertebrate cognitive complexity, Nat. Neurosci. 16 (2013) 16–24.
[32] R.A. Frank, N.H. Komiyama, T.J. Ryan, F. Zhu, T.J. O'Dell, S.G. Grant, NMDA receptors are selectively partitioned into complexes and supercomplexes during synapse maturation, Nat. Commun. 7 (2016) 11264.
[33] W. Liu, W. Wen, Z. Wei, J. Yu, F. Ye, C.H. Liu, et al., The INAD scaffold is a dynamic, redox-regulated modulator of signaling in the *Drosophila* eye, Cell 145 (2011) 1088–1101.
[34] J.F. Long, H. Tochio, P. Wang, J.S. Fan, C. Sala, M. Niethammer, et al., Supramodular structure and synergistic target binding of the N-terminal tandem PDZ domains of PSD-95, J. Mol. Biol. 327 (2003) 203–214.
[35] Y. Li, Z. Wei, Y. Yan, Q. Wan, Q. Du, M. Zhang, Structure of crumbs tail in complex with the PALS1 PDZ–SH3–GK tandem reveals a highly specific assembly mechanism for the apical crumbs complex, Proc. Natl. Acad. Sci. U. S. A. 111 (2014) 17444–17449.
[36] L. Pan, J. Chen, J. Yu, H. Yu, M. Zhang, The structure of the PDZ3–SH3-GuK tandem of ZO-1 protein suggests a supramodular organization of the membrane-associated guanylate kinase (MAGUK) family scaffold protein core, J. Biol. Chem. 286 (2011) 40069–40074.
[37] J. Nomme, A.S. Fanning, M. Caffrey, M.F. Lye, J.M. Anderson, A. Lavie, The Src homology 3 domain is required for junctional adhesion molecule binding to the third PDZ domain of the scaffolding protein ZO-1, J. Biol. Chem. 286 (2011) 43352–43360.
[38] J. Zhang, S.M. Lewis, B. Kuhlman, A.L. Lee, Supertertiary structure of the MAGUK core from PSD-95, Structure 21 (2013) 402–413.
[39] J.J. McCann, L. Zheng, D. Rohrbeck, S. Felekyan, R. Kuhnemuth, R.B. Sutton, et al., Supertertiary structure of the synaptic MAGuK scaffold proteins is conserved, Proc. Natl. Acad. Sci. U. S. A. 109 (2012) 15775–15780.
[40] M. Zeng, Y. Shang, Y. Araki, T. Guo, R.L. Huganir, M. Zhang, Phase transition in postsynaptic densities underlies formation of synaptic complexes and synaptic plasticity, Cell 166 (2016) 1163–1175 (e12).
[41] F. Ye, M. Zhang, Structures and target recognition modes of PDZ domains: recurring themes and emerging pictures, Biochem. J. 455 (2013) 1–14.
[42] M.W. Popp, J.M. Antos, H.L. Ploegh, Site-specific protein labeling via sortase-mediated transpeptidation, Curr Protoc Protein Sci. 56 (2009) 15.3.1–15.3.9.
[43] C.M. Petit, J. Zhang, P.J. Sapienza, E.J. Fuentes, A.L. Lee, Hidden dynamic allostery in a PDZ domain, Proc. Natl. Acad. Sci. U. S. A. 106 (2009) 18249–18254.
[44] D.A. Doyle, A. Lee, J. Lewis, E. Kim, M. Sheng, R. MacKinnon, Crystal structures of a complexed and peptide-free membrane protein-binding domain: molecular basis of peptide recognition by PDZ, Cell 85 (1996) 1067–1076.
[45] M.H. Roh, O. Makarova, C.J. Liu, K. Shin, S. Lee, S. Laurinec, et al., The Maguk protein, Pals1, functions as an adapter, linking mammalian homologues of crumbs and discs lost, J. Cell Biol. 157 (2002) 161–172.
[46] Y. Hata, S. Butz, T.C. Sudhof, CASK: a novel dlg/PSD95 homolog with an N-terminal calmodulin-dependent protein kinase domain identified by interaction with neurexins, J. Neurosci. 16 (1996) 2488–2494.
[47] B.S. Chen, J.A. Gray, A. Sanz-Clemente, Z. Wei, E.V. Thomas, R.A. Nicoll, et al., SAP102 mediates synaptic clearance of NMDA receptors, Cell Rep. 2 (2012) 1120–1128.
[48] S. Won, S. Incontro, R.A. Nicoll, K.W. Roche, PSD-95 stabilizes NMDA receptors by inducing the degradation of STEP61, Proc. Natl. Acad. Sci. U. S. A. 113 (2016) E4736–44.
[49] Y. Araki, M. Zeng, M. Zhang, R.L. Huganir, Rapid dispersion of SynGAP from synaptic spines triggers AMPA receptor insertion and spine enlargement during LTP, Neuron 85 (2015) 173–189.
[50] C.Y. Zheng, R.S. Petralia, Y.X. Wang, B. Kachar, R.J. Wenthold, SAP102 is a highly mobile MAGUK in spines, J. Neurosci. 30 (2010) 4757–4766.
[51] Y. Wang, H.G. Pascoe, C.A. Brautigam, H. He, X. Zhang, Structural basis for activation and non-canonical catalysis of the Rap GTPase activating protein domain of plexin, elife 2 (2013), e01279. .
[52] F. Delaglio, S. Grzesiek, G.W. Vuister, G. Zhu, J. Pfeifer, A. Bax, NMRPipe: a multidimensional spectral processing system based on UNIX pipes, J. Biomol. NMR 6 (1995) 277–293.